Proceedings of the 17th Pan-American Conference on Soil Mechanics and Geotechnical Engineering (XVII PCSMGE), and 2nd Latin-American Regional Conference of the International Association for Engineering Geology and the Environment (IAEG), La Serena Chile, 2024.

Nonlinear dynamic analysis of a large rockfill tailings dam.

Análisis dinámico no lineal de una presa de enrocado de gran altura para relaves.

Juan José Valdivia, Rolando Rojas, Carlos Huamán, José Ale
Mine Waste, WSP, Perú, juanjose.valdivia@wsp.com

ABSTRACT: This study assesses the seismic stability of a 260-meter high rockfill tailings dam in the Peruvian Andes through a nonlinear two-dimensional dynamic analysis. Given the extreme consequence classification of dam failure, simulations used the maximum credible earthquake (MCE) based on deterministic seismic hazard assessment (DSHA), employing three Seed acceleration time-history records—Tarapacá 2005, El Salvador 2001, and Valparaiso 1985—modified for spectral acceleration matching. The Plaxis 2D software and the Hardening Soil Small-Strain (HS Small) constitutive model for cyclic rockfill and tailings response were applied. A preliminary linear elastic free vibration analysis determined the fundamental frequency, aiding in Rayleigh damping parameter calculation. Geotechnical characterization, derived from laboratory testing using both large-scale direct shear and triaxial tests, facilitated rockfill behavior calibration. Results indicate that seismic displacements, settlements, and shear strains pose no threat to dam stability or induce global failure mechanisms.

KEYWORDS: Dynamic analysis, rockfill dam, cyclic response, large dam, finite element method.

1 INTRODUCTION

With the increasing need for tailings storage due to mining activities, the construction of Tailings Storage Facilities (TSFs) becomes a priority for Peru and the mining industry. Given the highly contaminating nature of tailings, the stability of TSFs must be assessed according to the most stringent international criteria and regulations (CDA 2019, ICMM 2020) to design a resilient structure over time, especially in seismically active regions like Peru. To achieve this goal, various approaches are available, with the downstream method of raising being the most physically stable for constructing large dams. Additionally, recommended configurations include raised dams with high-permeability rockfill on a competent rock foundation, deemed inherently stable (Cooke 1987, USSD 2014), as illustrated in the present case study.

Typically, slope stability of such dams is evaluated in terms of a pseudo-static safety factor, commonly set at 1.0 as minimum value, and limited seismic deformation. However, the nonlinear cyclic response of the materials complicates the analysis, and failure may not necessarily occur if this minimum design criterion is not met. Hence, more sophisticated analyses are necessary to determine performance and ascertain whether seismic-induced deformations are detrimental or within acceptable limits.

Therefore, nonlinear two-dimensional models, applied through the finite element method (FEM) under a dynamic stress-strain approach, are employed in this study to determine displacements and settlements following exposure to the design time-history record. These models require abundant input information from field investigations and laboratory tests to calculate the shear wave propagation velocity (Vs) and material properties based on chosen constitutive laws, such as the Hardening Soil Small-Strain model (Brinkgreve et al. 2014), which accounts for hysteretic behavior through dynamic parameters like the maximum reference shear modulus and material threshold shear strain.

Lastly, due to the lack of a concise criterion for concluding the stability of a rockfill dam based on calculated deformations from a numerical model, limits on settlements are often established as a percentage or the total value of the freeboard, as outlined in this study.

2 CASE STUDY

The case study involves a downstream-raised, high-permeability rockfill Tailings Storage Facility (TSF) with a height of approximately 260 m in the most critical analysis section. Two different scenarios for the downstream slope of 1.55H:1.0V and 1.60H:1.0V were modelled to study the variation of the shear strain values and contours along the downstream slope. This section features a filter and transition material on the upstream face to reduce pore pressure in the dam, causing seepage flow to emerge at the base of the structure. The specific location of the TSF is kept undisclosed due to confidentiality agreements.

The dam is founded on a competent rock foundation predominantly composed of limestones, siltstones, and shales with unconfined compressive strength (UCS) ranging between 100 to 120 MPa, and rock mass rating (RMR) between 50 and 70.

The 515.30 million cubic meters of low gradient deposited tailings consist of non-plastic silts that do not directly influence the dam's stability. However, they provide lateral confinement, contributing damping effects to reduce displacements occurring at the crest of the structure as shown in Figure 1.

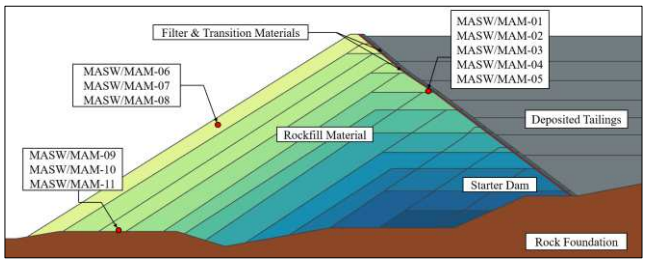

Figure 1. Downstream-raised rockfill TSF representative cross-section. Geophysical tests (MASW/MAM) are indicated, and the construction process is illustrated through different stages.

3 SEISMIC DESIGN CRITERIA

3.1 *Selection of seismic records and spectral matching*

The tectonic setting of Peru is characterized by the subduction of the Nazca Plate beneath the South American Plate at a rate of 7 to 9 cm/year (DeMets et al. 1990). Along the Peru subduction zone, two main types of seismicity can be identified: first, earthquakes occur in the seismically coupled interface between the Nazca and South American Plates (interface earthquakes), and second, seismicity is related to extension within the descending Nazca Plate (intraslab earthquakes).

In accordance with the deterministic seismic hazard analysis (DSHA) for this TSF, both types of seismicity could occur; however, there is a slight predominance of instraslab subduction earthquakes with a moment magnitude (Mw) of 7.9 and a focal depth ranging from 50 to 80 km. Based on this information, Tarapaca (2005), Valparaiso (1985), and El Salvador (2001) records were selected due to their compatibility with the seismological characteristics assessed in the DSHA.

Due to the dam consequence classification as "Extreme" (CDA 2019), it is imperative to spectrally match these three records to the uniform hazard spectrum corresponding to the maximum credible earthquake (MCE) calculated from the DSHA, which exhibits a peak ground acceleration (PGA) of 0.54g based on the 84th percentile of the results as shown in Figure 2.

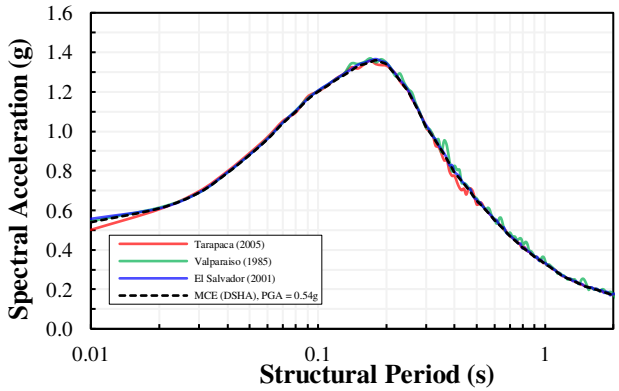

Figure 2. Results of the spectral match performed using the Al Atik & Abrahamson (2010) algorithm for the Tarapacá 2005, Valparaíso (1985) and El Salvador (2001) ground motions.

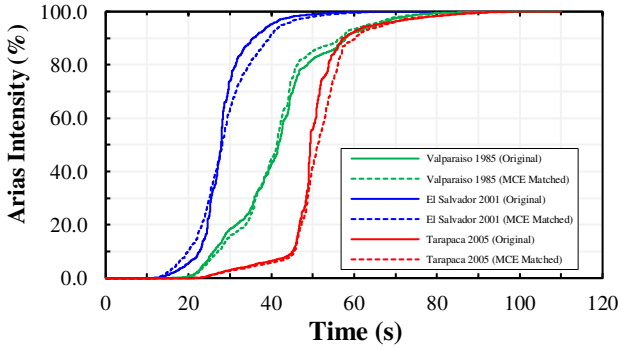

Figure 3. Comparison between the Arias intensity of the original and spectrally matched records to the Maximum Credible Earthquake (MCE).

Additionally, the results of spectral matching were compared in terms of the normalized Arias intensity to validate the quality of the procedure. Figure 3 depicts a strong correlation between the original time-histories and the matched ground motions.

3.2 *Acceleration time-histories*

The resulting records are shown in Figure 4 for the Valparaiso 1985 (interface ground motion), El Salvador 2001 and Tarapaca 2005 time-history (intraslab ground motions).

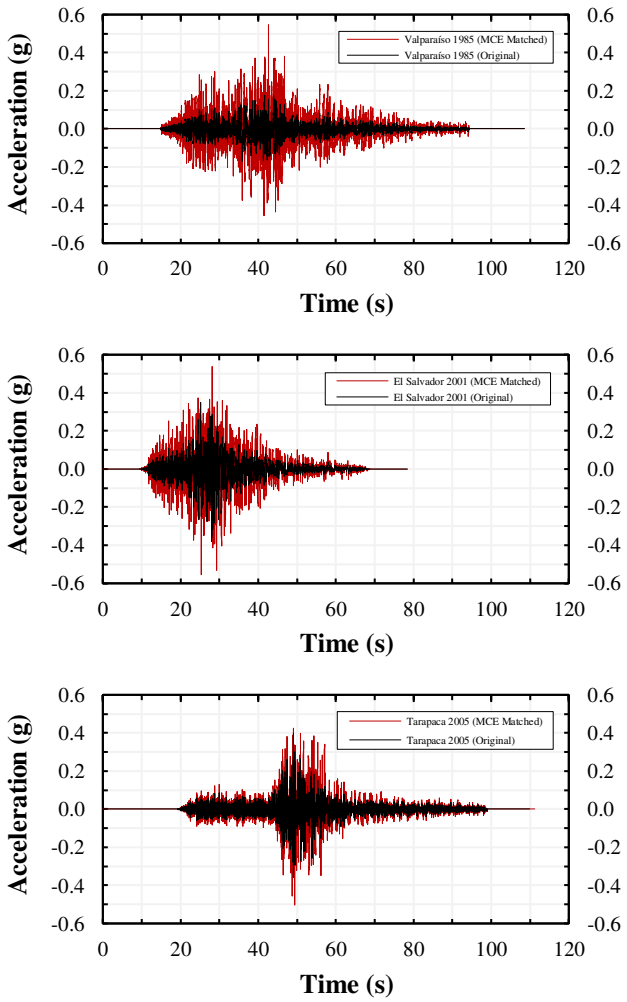

Figure 4. Matched acceleration time-histories for the Valparaíso (1985) El Salvador (2001) and Tarapacá (2005) ground motions.

3.3 *Acceptability criteria for seismic performance*

According to Swaisgood (2013), the same crest displacement value, normalized with respect to the dam height, can imply different degrees of damage caused by a seismic event, ranging from minor effects to serious damage in some studied cases.

Therefore, as an acceptance criteria for the seismic performance of the analyzed dam, it was established that the final settlement

experienced at the crest due to the seismic event must be less than the freeboard specified in the design (2.5 m). Additionally, it was determined that the filter and transition materials must not undergo a reduction of more than 50% of their original thickness to maintain the serviceability conditions of the earth structure.

4 GEOTECHNICAL CHARACTERIZATION

4.1 *In-situ testing*

To characterize the dynamic properties of the materials, MASW and MAM geophysical tests were conducted at locations specified in Figure 1 on the upstream and downstream slopes of the TSF, as well as on the surface of the competent rock foundation, where a minimum shear wave velocity of 200 m/s was determined for the rockfill material at surface and 1100 m/s for the competent rock foundation.

Given that the maximum particle size of the rockfill material is approximately 36", in-situ global gradation tests were performed, along with water replacement tests to determine the density of this material. For the fraction less than 3", the USCS classification is detailed as GP-GC with a fine fraction of up to 7% (plasticity index of 5). Density values range from 2.38 g/cm³ to 2.49 g/cm³, with an average water content of 2.74%.

4.2 *Laboratory testing*

Consolidated Drained Triaxial (CDTX) tests on large-scale specimens measuring 30x60 cm and 100x180 cm, and Direct Simple Shear (DSS) tests on 30x30 cm, were conducted to determine the friction angle and stress-strain curves of the rockfill material. For smaller maximum particle size gravels such as filter and transition materials (with maximum sizes of 3" and 12" respectively), smaller specimens (15x30 cm) were tested. These materials were classified as GW-GC and GP-GM, with fines content not exceeding 10% in either case.

Lastly, thickened tailings were classified as non-plastic silts (ML) based on laboratory tests, exhibiting fines content up to 53.3% and a specific gravity of solids of 2.77.

Table 1 summarizes the soil particle-size distribution of the rockfill, transition and filter materials considering both the in-situ and laboratory tests, as well as the tailings grain size distribution.

Table 1. Soil particle-size distribution of the construction materials

Classification	*Rockfill (%)*	*Transition (%)*	*Filter (%)*	*Tailings (%)*
Cobbles/Boulders	30-75	-	-	-
Gravel	15-50	70-85	70-85	-
Sand	6-20	20-30	30-50	45-50
Fines content*	2-7	6-9	6-7	50-55
Max. Particle Size	59"	12"	3"	#10
Plasticity Index	NP	NP	NP	NP

**Fines content defined as percent passing 0.075 mm (#200 sieve)*

5 NUMERICAL MODELING

5.1 *Constitutive model*

The Hardening Soil Small Strain constitutive model, (Brinkgreve et al., 2014), was used to characterize the stress-strain response of rockfill, filter, transition, and deposited tailings materials under both monotonic and cyclic loading. This model, designed to calculate the nonlinear material response, is formulated within an effective stress approach based on the Mohr-Coulomb failure criterion to compute the yield surface. It includes the implementation of a plastic potential function based on the dilatancy parameter to control volumetric deformations within the system.

As indicated by Sottile et al. (2021), during drained shear, the association between total axial strain and deviatoric stress in the soil is estimated using the hyperbolic model introduced by Duncan and Chang (1970). This model is then incorporated as a hardening rule in the HSS model. The stiffness in shear is governed by three parameters: "G_0" at small strain, "E_{50}" in the complete unloading-reloading path, and all three parameters utilize power-law expressions contingent upon the minor principal effective stress "σ'_3".

The HSS model incorporates dynamic parameters to simulate the hysteretic behavior of soils subjected to cyclic loads such as seismic events. This is achieved through the implementation of the low-strain shear modulus "G_0^{ref}" and the reference shear strain "$\gamma_{0,7}$" defined as the shear strain corresponding to 72.20% of the maximum reference shear modulus "G_0^{ref}" in the normalized curve of shear modulus degradation versus shear strain.

The linear elastic model was chosen to characterize the bedrock foundation since the shear wave velocities indicated that this material is rigid enough to assume this type of behavior.

5.2 *Strength parameters and reference elastic moduli*

The rockfill strength was estimated from large-scale and conventional triaxial tests and then plotted in a friction angle versus normal stress chart to compare it with reference minimum, average and maximum strength envelopes (Leps, 1970).

A logarithmic regression was conducted to calculate the curve that better represents the test results, as shown in Figure 5.

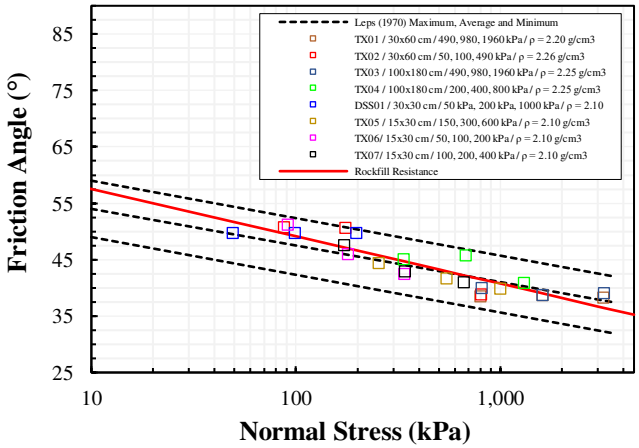

Figure 5. Friction angle versus normal stress of the TSF rockfill envelope compared with the curves from Leps (1970).

To estimate the reference elastic modulus at 50% of the maximum deviatoric stress "E_{50}^{ref}", stress-strain curves calculated from laboratory triaxial tests (TX01-TX07) were used and later adjusted to the curves obtained from the HSS model. On the other hand, the

oedometer modulus "E_{oed}^{ref}" was estimated using the following relation: $E_{50}^{ref} = E_{oed}^{ref}$ (Brinkgreve et al., 2014), which results in an adequate fit as shown in Figure 6. Finally, the criterion used to calculate the unloading-reloading elastic modulus was based on a better fit to the shear modulus reduction curves and damping ratio as a function of the shear strain, as will be discussed in section 5.3.

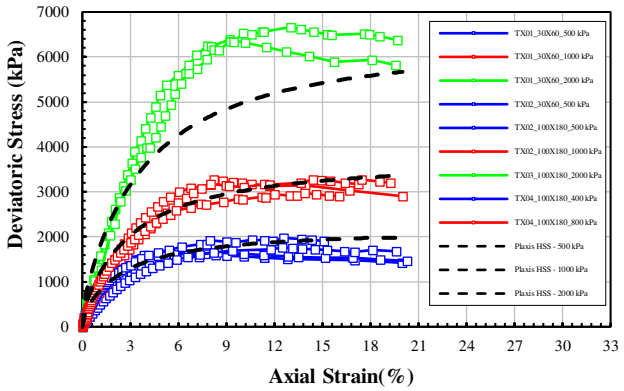

Figure 6. Comparison between stress-strain curves from the TXCD laboratory tests and the HSS constitutive model.

Since the depth of interest has confining stresses ranging from 100 kPa to 1200 kPa, the aim of the calibration was to fit the constitutive model stress-strain curves to better represent this range of stresses. Thus, Figure 6 illustrates a good correlation for the 400/500 kPa and 1000 kPa samples and shows a conservative strength from the HSS curve for the samples confined at 2000 kPa.

5.3 *Dynamic parameters*

The reference maximum shear modulus was calculated using geophysical MAM/MASW tests, prioritizing points near the analysis section for this study. Relation (1) from the HSS model was transformed into a shear wave distribution using elastic equations and then compared with the results of the geophysical tests, as well as with relation (2) (Seed and Idriss, 1970) which shows a good fit for a K2 = 120.

$$G_0 = G_0^{ref}\left(\frac{c\cdot\cos(\phi)-\sigma_3'\cdot\sin(\phi)}{c\cdot\cos(\phi)+p_{ref}\cdot\sin(\phi)}\right)^m \quad (1)$$

$$G_0 = 21.7\cdot K_{2-max}\cdot P_a\left(\frac{P'}{P_a}\right)^{0.5} \quad (2)$$

Where c, ϕ, σ_3', m and p_{ref} correspond to the soil cohesion, friction angle, stress-dependency parameter, effective confining stress, and reference pressure for the HSS constitutive law. Whereas K_{2-max}, P_a, and P'correspond to the shear modulus coefficient in the small-strain range, atmospheric pressure (101,3 kPa), and the mean effective stress for the Seed and Idriss (1970) equation.

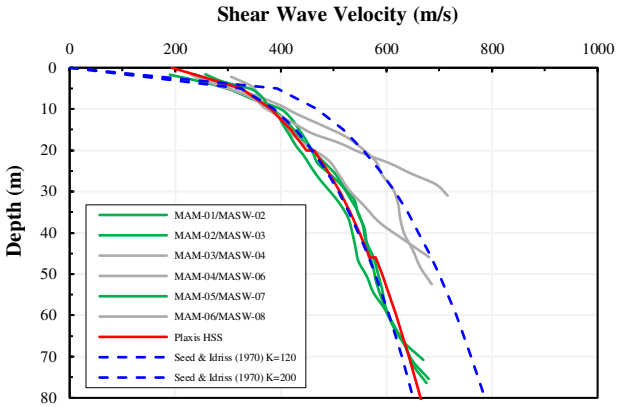

Figure 7. Comparison between shear wave velocities from the MAM/MASW tests and the HSS constitutive model.

As shown in Figure 7, the shear wave velocity profile of the model used for numerical simulation prioritizes the MAM/MASW tests located near the analysis section, specifically tests 02, 03, and 07. The curves were calibrated for a reference pressure of 100 kPa, enabling the calculation of the maximum shear modulus "G_0^{ref}" as 425 MPa. Additionally, the stiffness exponent "m" was estimated according to equation (1). This parameter is determined to be 0.50 for this case study, a value that is consistent with those reported in other studies for gravels, such as those by Von Soos (1991).

The threshold shear strain "$\gamma_{0,7}$" was estimated using reference empirical relations (Rollins, 2020) to calculate the normalized shear modulus degradation and damping amplification curves using a uniformity coefficient of Cu = 78 and different values of the effective vertical stress.

Using the reference modulus degradation curve for 100 kPa and the previously mentioned definition of this parameters, "$\gamma_{0,7}$" can be estimated as 0.008%.

Additionally, the unloading-reloading elastic modulus was calculated by calibrating the relationship between "G_0" and "G_{ur}" which determines the cut-off boundary for the shear modulus and damping ratio to seek a better fit with reference curves as shown in Figure 8.

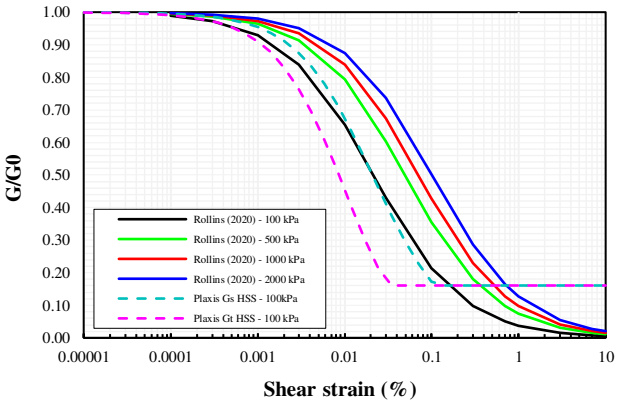

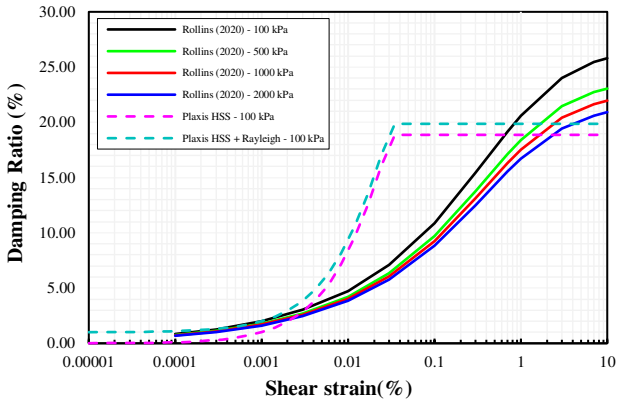

Figure 8. Calibration of the shear modulus degradation and damping amplification curves of the HSS model using Rollins (2020) equations.

The process showed that a value of E_{ur}^{ref} = 175 MPa led to a shear modulus reduction of approximately 16% of its small-strain reference value along with a maximum damping ratio of about 20% for the large-strain range.

Table 2. Material parameters used for the HSS model.

HSS Parameters	*Rockfill*	*Transition*	*Filter*	*Tailings*(**)
γ (kN/m³)	24	23.5	22.5	18
ϕ (°)	(*)	37	36	18
c (kPa)		5	15	0
ψ (°)	0	0	0	0
E_{50}^{ref} (MPa)	25	17.5	15	5
E_{oed}^{ref} (MPa)	25	8	6.5	5
E_{ur}^{ref} (MPa)	175	102	80	15
m	0.5	0.75	0.8	0.8
Rf	0.9	0.9	0.9	0.9
v_{ur}	0.28	0.28	0.28	0.30
K_0 (1-sin ϕ)	(*)	0.398	0.412	0.50
p_{ref} (kPa)	100	100	100	100

**The friction angle was discretized to simulate the resistance curve presented in Figure 5. Hence, K_0 varies accordingly.*
***Tailings were modeled using an undrained condition in which strength and stiffness are defined in terms of effective stresses*

5.4 *Geometry and finite elements mesh*

As a first step, the length of the finite elements was defined using the Lysmer & Kuhlemeyer (1969) criteria, which states that the element dimensions should be less than 1/8 of the maximum shear wavelength. Since surface displacements for the rockfill material are highly valuable, a V_{S30} = 384 m/s was calculated, and a maximum frequency of 15 Hz was set through the Fourier spectra from the different ground motions used in the present study, giving a maximum surface elements size of 3.21 m. Nevertheless, shear wave velocity increases with depth. Therefore, to optimize the numerical model, the finite element dimension increases accordingly.

Figure 10 shows the elements distribution used for the finite element model in PLAXIS, along with the dynamic boundary conditions considered. The discretization consisted of a total amount of 34 343 soil elements with 277 150 nodes with an average, minimum (surface rockfill layer) and maximum element size of 8.03 m, 3.17 m and 29.98 m, respectively. Thus, respecting the design criteria of Lysmer & Kuhlemeyer (1969).

Moreover, a set of four control points were spaced in the crest (P1: Downstream Crest and P2: Upstream Crest), and downstream slope (P3), to control deformations and amplification in the model.

5.5 *Sequence of analysis*

The modeling strategy included conducting a numerical analysis under static conditions, simulating the construction sequence of the dam to capture the stress state prior to the dynamic calculation phase. Given that the involved materials will operate in the range of large deformations under these conditions, it was deemed necessary to represent the stress-strain behavior of the rockfill by considering a reduction of the shear modulus to 10% of its maximum value calculated using the previously mentioned geophysical tests, namely, 42.5 MPa.

Furthermore, the variation of the friction angle of the dam body material was considered according to the strength curve outlined in Figure 5. This allowed for capturing a more realistic state of deformations and stresses as each construction stage was updated. Upon completion of the structure's construction, the calculated displacements were reset to evaluate only the effect of permanent deformations resulting from the dynamic load applied at the base of the finite element model.

Subsequently, the material parameters were updated in the preliminary dynamic phase as shown in Table 2, in order to calculate the fundamental vibration frequency of the rockfill dam. For this, an initial dynamic analysis was conducted without adding Rayleigh damping to the system, and the power spectra in terms of velocities were compared at the base and crest of the model. Figure 9 shows that the fundamental vibration frequency is f = 1.16 Hz, corresponding to a structural period of approximately Ts = 0.86 s.

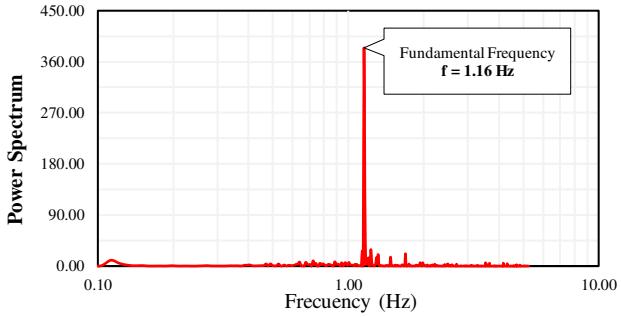

Figure 9. Rockfill dam's fundamental vibration frequency.

Once this frequency has been obtained, the Rayleigh parameters can be determined using, in addition, the characteristic frequencies of each earthquake analyzed (Hudson et al., 1994).

The subsequent step consisted of viscous damping being incorporated into the finite element model to enable the execution of the final analyses. This process allowed for the determination of the permanent deformations induced by the Valparaíso 1985, Tarapacá 2005, and El Salvador 2001 earthquakes.

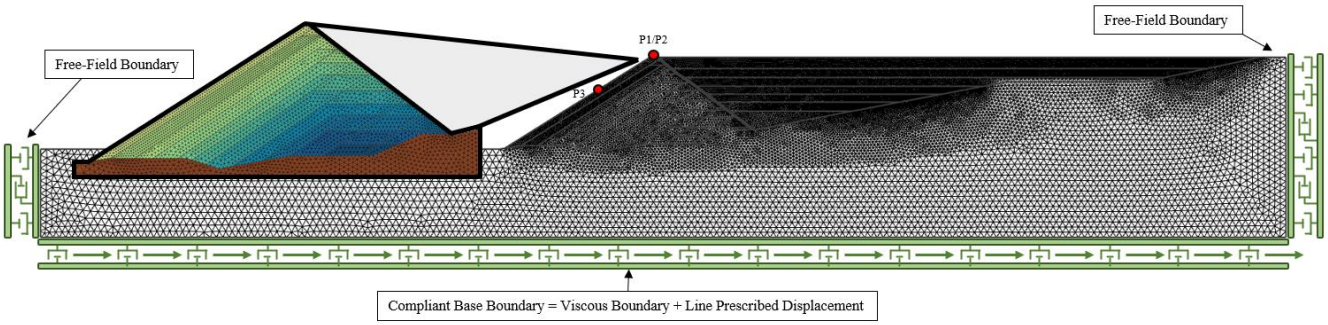

Figure 10. Finite element mesh, boundary conditions and control points.

Table 3 summarizes the Rayleigh parameters implemented in the dynamic model.

Table 3. Rayleigh parameters for viscous damping.

Material	α_R	β_R	*Damping Ratio (%)*
Transition	0.0885	0.8120 x 10^{-3}	1.0
Filter			1.0
Rockfill			1.0
Tailings			3.0

6 Results

6.1 *1.55H:1.0V Design Slope*

Since the analyses were conducted under drained conditions, the results are presented in the format of horizontal and vertical displacements, and shear strains developed in the two-dimensional model, focusing mainly on the points strategically distributed within the dam body.

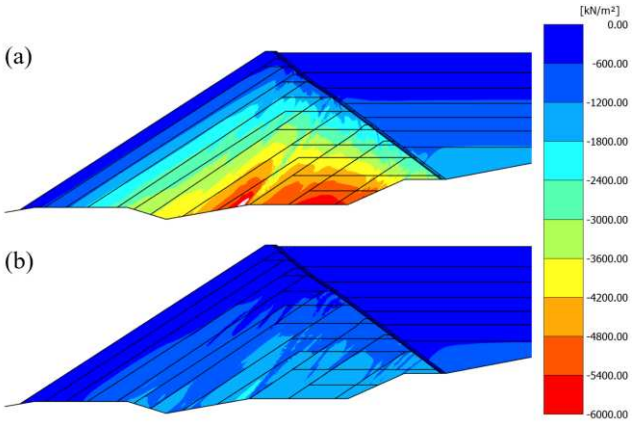

Figure 11. Cartesian effective stresses σ'$_{yy}$ (a) and σ'$_{xx}$ (b) at the end of the construction process.

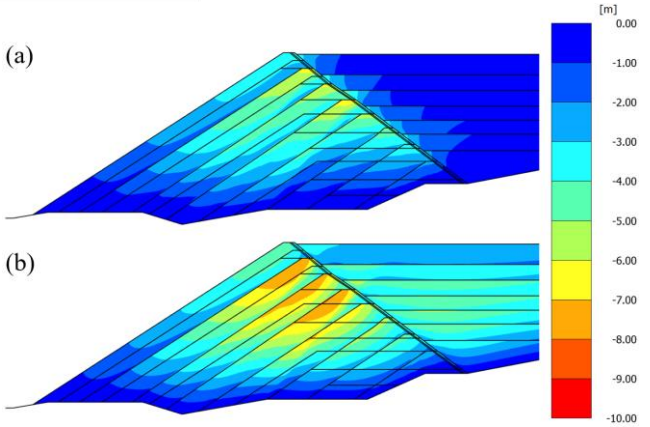

Figure 12. Sum phase displacements of the horizontal (a) and vertical (b) component at the end of the construction process.

As previously described, capturing the initial static state of the model accurately is essential to ensure the correct distribution of HSS model parameters as shown in Figure 11 and Figure 12. As the next step, the results of horizontal deformation (Figure 13), settlements (Figure 14), and total shear strains (Figure 15) along the numerical model are presented.

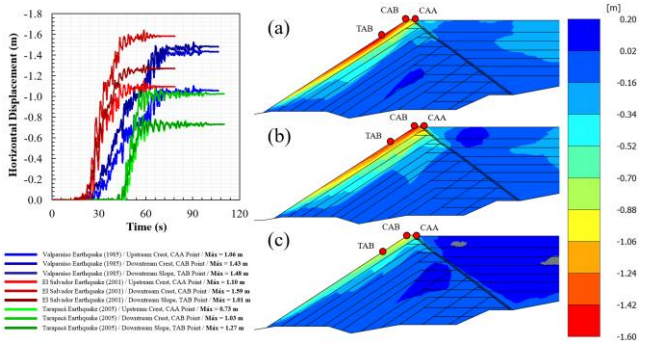

Figure 13. 1.55H:1.0V Slope: Horizontal seismic induced displacements for the (a) Valparaíso (1985), (b) El Salvador (2001) and (c) Tarapacá (2005) earthquakes.

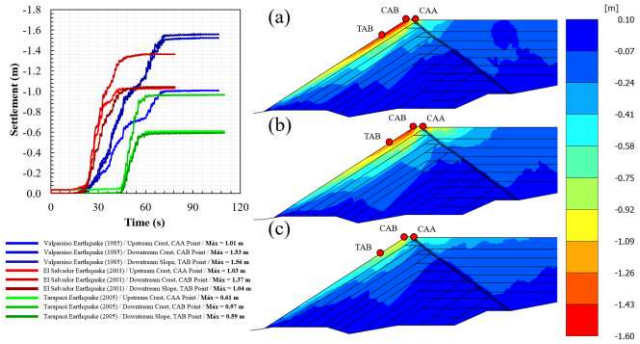

Figure 14. 1.60H:1.0V Slope: Vertical seismic induced displacements for the (a) Valparaíso (1985), (b) El Salvador (2001) and (c) Tarapacá (2005) earthquakes.

The Plaxis2D model estimated a range of horizontal displacements at the crest of the dam from 0.73 m to 1.59 m corresponding to the Tarapaca (2005) and the El Salvador (2001) earthquakes, respectively. In addition, the values of seismic induced settlements range from 0.61 m to 1.56 m corresponding to the Tarapaca (2005) and the Valparaiso (1985) earthquakes, severally.

The filter and transition material suffered extension displacements of approximately 30 cm, which can be considered acceptable since the degradation of this components does not reach the 50% limit.

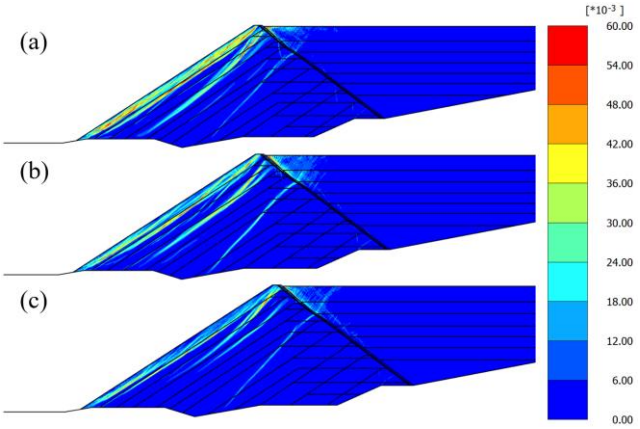

Figure 15. 1.55H:1.0V Slope: Total seismic induced shear strains for the (a) Valparaiso (1985), (b) El Salvador (2001) and (c) Tarapaca (2005) earthquakes.

The concentration of total shear strains is most notorious throughout the first 40 m of depth at the downstream slope of the model, reaching values in the range of 3% to a maximum of 6%. However, these shear strains contours are not continuous, hence there is no evidence of a failure mechanism developing in the dam.

6.2 *1.60H:1.0V Design Slope*

Similar simulations were run changing the downstream slope of the tailings dam to 1.60H:1.0V in order to assess the effects of the geometric design to the seismic response in terms of displacements, settlements and shear strains as shown in Figure 16 to Figure 18.

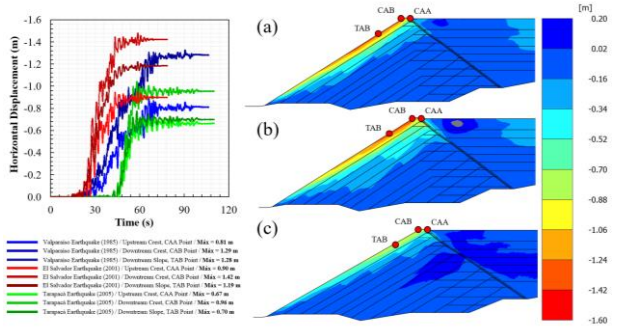

Figure 16. 1.60H:1.0V Slope: Horizontal seismic induced displacements for the (a) Valparaíso (1985), (b) El Salvador (2001) and (c) Tarapacá (2005) earthquakes.

As expected, displacements were lower, reaching a difference of 10.7% for the horizontal component and 14.7% for the vertical component for the maximum value calculated in each model. Thus, evidencing the great impact of a slight variation in the downstream slope geometry for this type of dams.

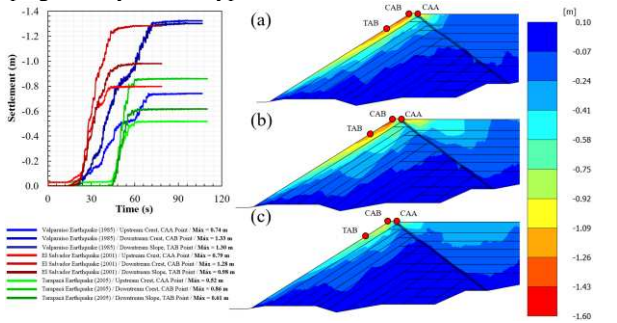

Figure 17. 1.60H:1.0V Slope: Vertical seismic induced displacements for the (a) Valparaiso (1985), (b) El Salvador (2001) and (c) Tarapacá (2005) earthquakes.

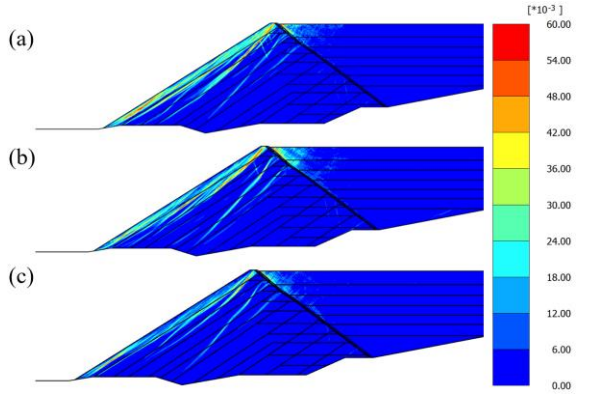

Figure 18. 1.60H:1.0V Slope: Total seismic induced shear strains for the (a) Valparaíso (1985), (b) El Salvador (2001) and (c) Tarapacá (2005) earthquakes.

Finally, the maximum value of shear strains reduces to approximately 5% with the change of the downstream slope. Thus, preventing a major degradation of the dynamic properties of the rockfill material.

7 CONCLUSIONS

A plane-strain bidimensional dynamic analysis was performed to evaluate the performance of a 260 meter-high rockfill tailings dam subjected to three ground motion records that were selected according to the seismic hazard analysis. A non-linear constitutive model that takes the hysteretic behavior of the material and the elastic/shear modulus variation as a function of the confining pressure was calibrated to simulate the seismic response of the rockfill and tailings present in the model.

Despite reaching maximum values of 6% total shear strain, the results showed that no evident failure mechanisms are developed at the end of the simulation of any of the three ground motions applied at the base of the model. Maximum values of horizontal displacement and settlement of 1.59 m and 1.56 m were computed. Thus, conservating 38% of the free-board and maintaining the operational conditions of the dam.

A slight variation on the downstream slope angle of a large rockfill tailings dam resulted in a reduction of horizontal and vertical displacement, as well as shear strains on the model, reaching up to 14.7% less settlement on the downstream point at the top of the crest for the present study.

The results of this investigation are only applicable for drained conditions of the rockfill material. Additionally, further research should be conducted in order to assess the liquefaction potential of the tailings beach near the crest of the dam to assess the influence of tailing strength reduction on the maximum settlement and displacement on crest.

Finally, despite having a good performance to simulate the hysteretic behavior of the rockfill, the HSS constitutive model overdamps the numerical model and does not allow for the shear modulus to degrade to its minimum values according to the Rollins (2020) curves. Hence, underestimating displacements within the FE mesh. This is why a further study should be conducted with other constitutive models to evaluate this effect on the seismic response of the tailings dam.

8 ACKNOWLEDGEMENTS

Authors would like to thank WSP team for the support to conduct this study.

9 REFERENCES

Al Atik L, Abrahamson N. 2010. An Improved Method for Nonstationary Spectral Matching. Earthquake Spectra. 26(3) :601-617.

Benz T. 2007. Small-strain stiffness of soils and its numerical consequences. PhD Thesis, Institute of Geotechnical Engineering, Universitat Stuttgart.

Brinkgreve, R.B.J.; Engin E. and Swolfs W.M. 2014. Plaxis 2D Anniversary Edition, Plaxis bv.

CDA. 2019. Application of Dam Safety Guidelines to Mining Dams. Canadian Dam Association.

Cooke J.B and Sherard J.L. 1987. Concrete-Face Rockfill Dam : II. Design, Journal of Geotechnical Engineering, Volume 113, No. 10, American Society of Civil Engineers.

DeMets, C., Gordon, R.G., Argus, D.F. and Stein, S. 1990. Current plate motions. Geophysical Journal International, 101: 425-478.

Duncan, J.M. and Chang, C.M. 1970. Nonlinear analysis of stress and strain in soils. Journal of Soil Mechanics and Foundations Division, ASCE, 96(SM5), 1629-1653.

Hudson M., Idriss I.M. y Beikae M. (1994). QUAD4M: A computer program to evaluate the seismic responde of soil structures using finite element procedures and incorporating a compliant base. Center for geotechnical modeling, University of California, Davis.

ICMM. 2020. Global Industry Standard on Tailings Management, International Council on Mining and Metals.

ICOLD. 2014. Selecting seismic parameters for large dams guidelines, Bulletin 148, International Commission on Large Dams.

Leps T. 1970. Review of Shearing Strenght of Rockfill. Journal of the Soil Mechanics and Foundation Division. 94 (4).

Lysmer. J. and Kuhlemeyer, R.L. 1969. Finite Dynamic Model for Infinite Media. Journal of Engineering Mechanics Division, 95, 859-878.

Rollins, K.M., Singh M. and Roy J 2020. Simplified equations for shear-modulus degradation and damping of gravels. Journal of Geotechnical and Geoenvironmental Engineering, Volume 146, Issue 9.

Seed, H. B., and Idriss, I. M. 1970. Soil Moduli and Damping Factors for Dynamic Response Analyses. Technical Report EERRC-70-10, Berkeley, California : University of California.

Sottile M.G, Cueto I.A., Sfrisso A.O., Ledesma O.N. and Lizacano A. 2021. Flow liquefaction triggering analyses of a Tailings Storaga Facility by means of a simplified numerical procedure. Proceedings of the 20th International Conference on Soil Mechanics and Geotechnical Engineering.

Swaisgood, J. R. 2013. Predicting dam deformation caused by earthquakes – an update. ASDSO Dam Safety Conference. Rhode Island.

United States Society on Dams (2014), Observed Performance of Dams During Earthquakes, Volume III, February 2014.

Von Soos, P. 1991. Grundbataschenbuch. Part 4. Ernst & Sohn, Berlin. 80, 117